RSC Advances

PAPER

Thermal analysis of ultrathin, compliant sensors for characterization of the human skin

Cite this: *RSC Adv.*, 2014, **4**, 5694

Zuguang Bian,[ab] Jizhou Song,*[c] R. Chad Webb,[d] Andrew P. Bonifas,[d] John A. Rogers[d] and Yonggang Huang*[be]

Recent work establishes that ultrathin, stretchable sensors can enable high precision thermal characterization of the skin, with capabilities for spatial mapping, in forms that avoid irritation, thermal or mechanical loads on natural behaviors, or motion artifacts. The results have potential for use in cardiovascular screening, skin hydration sensing, and local skin heating and thermal therapy. A theoretical framework for understanding the thermal behavior of these types of sensors is critically important for interpreting the data and identifying optimized designs. This paper presents an analytical model, validated by the finite element method and experiments, for this purpose. The sensor temperature is obtained analytically in terms of material and geometric parameters. A scaling law for the sensor response time shows that the normalized time depends only on the normalized sensor location and normalized thermal properties. A simple, analytic formula for the response at long times is also obtained. The results provide strategies for reducing the sensor response time and thereby for improving the device performance.

Received 21st September 2013
Accepted 17th December 2013

DOI: 10.1039/c3ra45277h

www.rsc.org/advances

1. Introduction

Skin temperature changes are correlated with physical, mental, and cardiovascular functions of the human body.[1–4] Several approaches have been established for skin temperature measurement and monitoring. One uses infrared cameras to noninvasively monitor human skin temperature.[5,6] This approach can obtain high resolution measurements but it is limited to clinical trials with immobilized patients due to the motion restrictions associated with the camera and its cost. Other schemes use temperature sensors, mounted to the skin with flexible adhesive pads.[7,8] Although these sensors have simple designs, none offers desirable capabilities such as temperature mapping over large areas (>1 cm^2), pathways to eliminate the occlusive nature of the adhesive mounting pads, or associated thermal loads on the natural behaviors of the skin. Recently developed technologies, sometimes referred to as epidermal electronics, open avenues to overcome these limitations, with classes of skin mounted sensors that have the ability to bend, twist, and stretch like human skin, with minimal effect on natural processes.[9]

Webb *et al.* developed stretchable epidermal sensors for thermal characterization of human skin and achieved high resolution skin temperature measurements with mapping and motion capabilities.[1] The temperature sensor, which can act simultaneously as a heater element, is made of gold, lithographically defined into interwoven serpentine traces 20 μm wide, and 50 nm thick, with a total length 21 mm. Changes in electrical resistance enable measurements of temperature. Such sensors, embedded in a layer of polyimide, are integrated onto a thin, low elastic modulus (60 μm thick, 30 kPa) elastomeric sheet. A cross-sectional view of the temperature sensor appears in Fig. 1. Measurements are performed with the sensors in intimate, conformal contact with the skin.

The thermal properties of these types of sensors are important to their operation. To obtain an accurate measurement of temperature change (below 1 Hz),[1] the response time, which is defined as the time for the sensor to reach 90% of the final

[a]*Ningbo Institute of Technology, Zhejiang University, Ningbo 315100, China*
[b]*Department of Civil and Environmental Engineering and Department of Mechanical Engineering, Northwestern University, Evanston, IL 60208, USA. E-mail: y-huang@northwestern.edu*
[c]*Department of Engineering Mechanics and Soft Matter Research Center, Zhejiang University, Hangzhou 310027, China. E-mail: jzsong@gmail.com*
[d]*Department of Materials Science and Engineering, University of Illinois, Urbana, IL 61801, USA*
[e]*Center for Engineering and Health, and Skin Disease Research Center, Northwestern University, Evanston, IL 60208, USA*

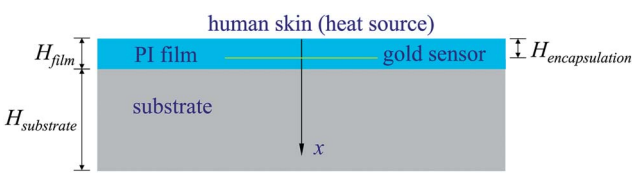

Fig. 1 Cross-sectional illustration of the temperature sensor.

temperature increase, must be small enough to ensure fast response. Experimental characterization of the response time is carried out by dropping a warm glycol droplet, which has similar thermal properties to skin, onto the sensor.[1] Such data indicate that the sensor response time is ~10 ms depending on the material and geometric parameters.

For better understanding of the device operation and identifying improved device designs and fabrication strategies, an analytical model, validated by experiments and finite element method (FEM), is developed for the thermal response. It should be noted that the current model is for this new type of compliant human skin sensor, which has not been studied before. There exist several thermal models, but none of them can be applied here. The sensor temperature is obtained analytically and a scaling law is established for response time. The results establish design guidelines for optimized performance.

2. Results and discussion

Fig. 1 shows a schematic illustration of a stretchable epidermal sensor, encapsulated by a top layer of PI (thickness $H_{\text{encapsulation}}$). Below the sensor is another PI layer. The total thickness of the PI film is denoted by H_{film} (Fig. 1). The sensor, embedded in the film, is attached to an elastomeric solaris substrate (thickness $H_{\text{substrate}}$). In the experiment[1] the embedded sensor (and elastomeric substrate) contacts the human skin (or a heat source). The skin has a temperature T_0 above the ambient.

The PI film has the thermal conductivity $k_{\text{film}} = 0.12\ \text{W m}^{-1}\ \text{K}^{-1}$ and thermal diffusivity $\alpha_{\text{film}} = 7.75 \times 10^{-8}\ \text{m}^2\ \text{s}^{-1}$, while the solaris substrate has $k_{\text{substrate}} = 0.186\ \text{W m}^{-1}\ \text{K}^{-1}$ and $\alpha_{\text{substrate}} = 1.08 \times 10^{-7}\ \text{m}^2\ \text{s}^{-1}$.[10,11] In the experiment, their thicknesses are $H_{\text{film}} = 3.6\ \mu\text{m}$ and $H_{\text{substrate}} = 60\ \mu\text{m}$, respectively.[1]

2.1 Analytic model

The sensor in the experiment is very thin (*e.g.*, ~50 nm), but its thermal conductivity and diffusivity are more than 1600 times larger than those of PI.[10,12] Overall, the sensor has a negligible effect on the temperature distribution in the film (and the entire system).

The film thickness (*e.g.*, 3.6 μm) is much smaller than its width (70 μm) and length (~1 mm) such that the heat flux is mainly along the thickness direction. The temperature increase T (from the ambient temperature) in the film and substrate can then be represented by a one-dimensional heat transfer model[13]

$$\frac{\partial T}{\partial t} - \alpha \frac{\partial^2 T}{\partial x^2} = 0, \tag{1}$$

where α is the thermal diffusivity, t is time, and x is the coordinate along the thickness direction with its origin on the top surface of PI (Fig. 1). Contact with the human skin gives a constant temperature increase T_0 at the top,

$$T|_{x=0} = T_0. \tag{2}$$

Continuity of temperature and heat flux across the film/substrate interface requires

$$T|_{x=H_{\text{film}}-0} = T|_{x=H_{\text{film}}+0} \text{ and } -k_{\text{film}} \left.\frac{\partial T}{\partial x}\right|_{x=H_{\text{film}}-0} = -k_{\text{substrate}} \left.\frac{\partial T}{\partial x}\right|_{x=H_{\text{film}}+0}, \tag{3}$$

where k is the thermal conductivity. Prior analytical and numerical studies have shown that the natural convection at the bottom surface of the substrate has a negligible effect and can be approximated by a thermal isolation condition[14]

$$\left.\frac{\partial T}{\partial x}\right|_{x=H_{\text{film}}+H_{\text{substrate}}} = 0. \tag{4}$$

The initial condition is

$$T|_{t=0} = 0. \tag{5}$$

The Laplace transform $\tilde{T}(x, s) = \int_0^\infty T(x, t)\exp(-st)\mathrm{d}t$ of eqn (1), with the initial condition (5), leads to the solution $\tilde{T} = B_{\text{film}}\exp\left(x\sqrt{s/\alpha_{\text{film}}}\right) + C_{\text{film}}\exp\left(-x\sqrt{s/\alpha_{\text{film}}}\right)$ for the film and $\tilde{T} = B_{\text{substrate}}\exp\left(x\sqrt{s/\alpha_{\text{substrate}}}\right) + C_{\text{substrate}}\exp\left(-x\sqrt{s/\alpha_{\text{substrate}}}\right)$ for the substrate, where B_{film}, C_{film}, $B_{\text{substrate}}$ and $C_{\text{substrate}}$ are constants to be determined by the Laplace transform of boundary and continuity conditions in eqn (2)–(4). The transformed temperature increase in the film ($0 \le x \le H_{\text{film}}$) is then given by

$$\tilde{T} = \frac{T_0}{s}\frac{\cosh\left[\left(H_{\text{film}} - x\right)\sqrt{\frac{s}{\alpha_{\text{film}}}}\right] + \beta\tanh\left(H_{\text{substrate}}\sqrt{\frac{s}{\alpha_{\text{substrate}}}}\right)\sinh\left[\left(H_{\text{film}} - x\right)\sqrt{\frac{s}{\alpha_{\text{film}}}}\right]}{\cosh\left(H_{\text{film}}\sqrt{\frac{s}{\alpha_{\text{film}}}}\right) + \beta\tanh\left(H_{\text{substrate}}\sqrt{\frac{s}{\alpha_{\text{substrate}}}}\right)\sinh\left(H_{\text{film}}\sqrt{\frac{s}{\alpha_{\text{film}}}}\right)}, \tag{6}$$

where

$$\beta = \frac{k_{\text{substrate}}}{k_{\text{film}}}\sqrt{\frac{\alpha_{\text{film}}}{\alpha_{\text{substrate}}}} \tag{7}$$

represents the ratio of film and substrate thermal properties.

As shown in the Appendix, the inverse Laplace transform of eqn (6) gives

$$\frac{T}{T_0} = 1 - 2\sum_{m=1}^{\infty}\left(\overline{H}\lambda_m + \frac{\beta\lambda_m}{\cos^2\lambda_m + \beta^2\sin^2\lambda_m}\right)^{-1} \times \sin\left(\overline{H}\lambda_m\frac{x}{H_{\text{film}}}\right)\exp\left(-\overline{H}^2\lambda_m{}^2\frac{\alpha_{\text{film}}t}{H_{\text{film}}{}^2}\right), \tag{8}$$

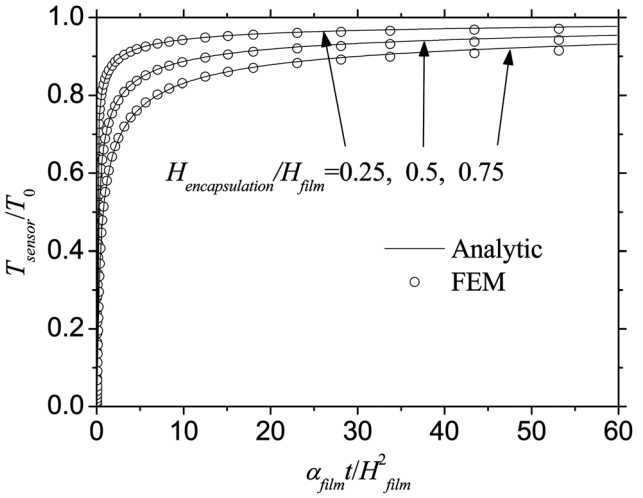

Fig. 2 The normalized temperature increase *versus* the normalized time, where the thickness $H_{\text{film}} = 3.6$ μm and $H_{\text{substrate}} = 60$ μm.

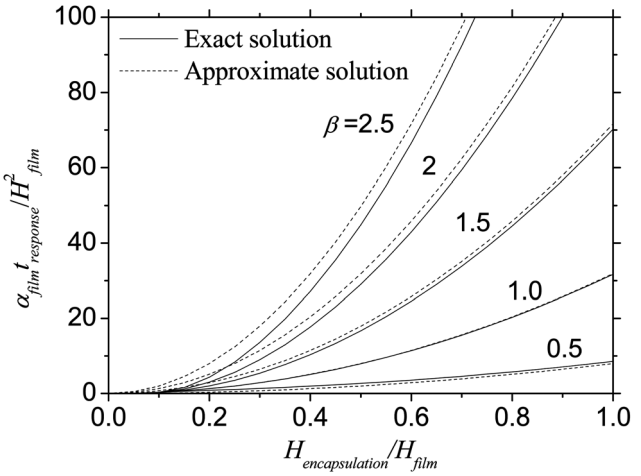

Fig. 3 The normalized sensor response time *versus* the normalized sensor location from the exact solution eqn (12) and approximate solution eqn (13).

where

$$\overline{H} = \sqrt{\frac{\alpha_{\text{substrate}}}{\alpha_{\text{film}}}}\,\frac{H_{\text{film}}}{H_{\text{substrate}}} \tag{9}$$

represents the normalized film-to-substrate thickness ratio, and λ_m ($m = 1, 2, 3,\ldots$) are the positive roots of the following equation

$$\cos\lambda_{\text{m}}\cos(\bar{H}\lambda_{\text{m}}) - \beta\sin\lambda_{\text{m}}\sin(\bar{H}\lambda_{\text{m}}) = 0. \tag{10}$$

The temperature increase of the sensor, T_{sensor}, which is the same as the temperature increase in the film at the same location $x = H_{\text{encapsulation}}$, can be obtained as

$$\frac{T_{\text{sensor}}}{T_0} = 1 - 2\sum_{m=1}^{\infty}\left(\overline{H}\lambda_m + \frac{\beta\lambda_m}{\cos^2\lambda_m + \beta^2\sin^2\lambda_m}\right)^{-1} \times \sin\left(\overline{H}\lambda_m\frac{H_{\text{encapsulation}}}{H_{\text{film}}}\right)\exp\left(-\overline{H}^2\lambda_m{}^2\frac{\alpha_{\text{film}}t}{H_{\text{film}}{}^2}\right). \tag{11}$$

Fig. 2 shows the normalized temperature increase T_{sensor}/T_0 *versus* the normalized time $\alpha_{\text{film}}t/H_{\text{film}}{}^2$. The normalized sensor locations are $H_{\text{encapsulation}}/H_{\text{film}} = 0.25$, 0.5 and 0.75. As the encapsulation layer becomes thinner (*i.e.*, smaller $H_{\text{encapsulation}}/H_{\text{film}}$), T_{sensor} approaches T_0 much more rapidly. The result is a reduced response time, as discussed in Section 2.2. The finite element method, which accurately accounts for the layout of the sensor system (*e.g.*, finite thickness and width of the gold sensor embedded in the PI film), and the heat convection condition at the bottom surface of the substrate, is also used. The numerical results, also shown in Fig. 2, agree with the analytic solution in eqn (11).

2.2 Sensor response time

The sensor response time is defined as the time at which the sensor temperature increase T_{sensor} reaches 90% of T_0. For $H_{\text{encapsulation}} = 2.4$ μm and other parameters described in the beginning of Section 2, the response time predicted by eqn (11) is 3.9 ms, which agrees well with the experimental measurement, 4.2 ms. A small sensor response time is important for accurate measurement capability.[1]

The normalized sensor response time $\alpha_{\text{film}}t/H_{\text{film}}{}^2$ is determined from eqn (11) and $T_{\text{sensor}}/T_0 = 0.9$. In general, the substrate is much thicker than the film (*e.g.*, $H_{\text{substrate}} = 60$ μm and $H_{\text{film}} = 3.6$ μm) such that it can be approximated as infinite. The temperature increase of the sensor in eqn (11) then becomes

$$\frac{T_{\text{sensor}}}{T_0} = 1 - \frac{2\beta}{\pi}\int_0^{\infty}\frac{1}{\xi\left(\cos^2\xi + \beta^2\sin^2\xi\right)}\sin\left(\frac{H_{\text{encapsulation}}}{H_{\text{film}}}\xi\right) \times \exp\left(-\frac{\alpha_{\text{film}}t}{H_{\text{film}}{}^2}\xi^2\right)\mathrm{d}\xi. \tag{12}$$

For $T_{\text{sensor}}/T_0 = 0.9$, the above equation gives the normalized sensor response time, $\alpha_{\text{film}}t_{\text{response}}/H_{\text{film}}{}^2$, that depends only on the normalized sensor location $H_{\text{encapsulation}}/H_{\text{film}}$ and thermal properties β. Fig. 3 shows $\alpha_{\text{film}}t_{\text{response}}/H_{\text{film}}{}^2$ *versus* $H_{\text{encapsulation}}/H_{\text{film}}$ for several values of β. The normalized sensor response time decreases with $H_{\text{encapsulation}}/H_{\text{film}}$ and β, which suggests to achieve fast response of the temperature sensor by reducing the encapsulation layer thickness or β.

For the normalized sensor response time $\alpha_{\text{film}}t_{\text{response}}/H_{\text{film}}{}^2 \gg 1$, the integral in eqn (12) can be obtained analytically to give

$$t_{\text{response}} = (1-0.9)^{-2}\frac{H_{\text{encapsulation}}{}^2}{\pi\alpha_{\text{substrate}}}\left(\frac{k_{\text{substrate}}}{k_{\text{film}}}\right)^2, \tag{13}$$

where the coefficient $(1-0.9)^{-2}$ is for T_{sensor} reaching 90% of T_0, and can be changed to $(1-0.95)^{-2}$ and $(1-0.99)^{-2}$ for other choices of T_{sensor} reaching 95% and 99% of T_0, respectively. The requirement $\alpha_{\text{film}}t_{\text{response}}/H_{\text{film}}{}^2 \gg 1$ then becomes $(H_{\text{encapsulation}}/H_{\text{film}})^2(\alpha_{\text{film}}/\alpha_{\text{substrate}})(k_{\text{substrate}}/k_{\text{film}})^2 \gg \pi(1-0.9)^2$. Eqn (13) shows that the sensor response time is proportional to the square of the encapsulation layer thickness (and also depends on the

film and substrate properties). Fig. 3 also shows the sensor response time in eqn (13), which agrees remarkably well with the accurate solution obtained numerically in eqn (12). Eqn (13) provides a very simple, but accurate, estimate of the sensor response time, and is useful for the optimal design of temperature sensors.

3. Conclusion

We have developed an analytical model for thermal characterization of stretchable epidermal sensors. The model is validated by FEM and experiments. The sensor temperature is obtained analytically which yields a simple scaling law for the normalized sensor response time $\alpha_{\text{film}}t_{\text{response}}/H_{\text{film}}{}^2$ in terms of two non-dimensional parameters: the normalized sensor location $H_{\text{encapsulation}}/H_{\text{film}}$ and the normalized thermal properties $\beta = \frac{k_{\text{substrate}}}{k_{\text{film}}}\sqrt{\frac{\alpha_{\text{film}}}{\alpha_{\text{substrate}}}}$. Small $H_{\text{encapsulation}}/H_{\text{film}}$ and β are helpful to reduce the sensor response time. For relative large $\alpha_{\text{film}}t_{\text{response}}/H_{\text{film}}{}^2$, a simple, analytic formula for the sensor response time is obtained, which is proportional to the square of the encapsulation layer thickness. These results provide useful design guidelines to improve sensor design and fabrication.

Appendix

The temperature increase is obtained by the inverse Laplace transform[15] $T = \frac{1}{2\pi i}\int_{\gamma-\infty i}^{\gamma+\infty i}\tilde{T}\exp(st)\mathrm{d}s$ of eqn (6), where $i = \sqrt{-1}$ and γ is a real constant that exceeds the real part of all the poles of $\tilde{T}$. The integrand $\tilde{T}\exp(st)$ has simple poles that give a vanishing denominator of the integrand in the complex plane of s. One pole is $s = 0$, and the others satisfy

$$\cosh\left(H_{\text{film}}\sqrt{\frac{s}{\alpha_{\text{film}}}}\right) + \beta\tanh\left(H_{\text{substrate}}\sqrt{\frac{s}{\alpha_{\text{substate}}}}\right) \times \sinh\left(H_{\text{film}}\sqrt{\frac{s}{\alpha_{\text{film}}}}\right) = 0, \tag{A1}$$

which gives the poles $s = -\alpha_{\text{film}}(\bar{H}/H_{\text{film}})^2\lambda_m{}^2$ $(m = 1, 2,\ldots)$, where λ_m is the positive root of eqn (10). The residual at $s = 0$ is 1. The residue at other poles is given by

$$-2\left(\bar{H}\lambda_m + \frac{\beta\lambda_m}{\cos^2\lambda_m + \beta^2\sin^2\lambda_m}\right)^{-1}\sin\left(\bar{H}\lambda_m\frac{x}{H_{\text{film}}}\right) \times \exp\left(-\bar{H}^2\lambda_m{}^2\frac{\alpha_{\text{film}}t}{H_{\text{film}}{}^2}\right). \tag{A2}$$

The Cauchy's residual theorem[8] then gives the temperature increase in eqn (11).

Acknowledgements

Z.B. acknowledges the supports from Zhejiang Provincial Natural Science Foundation of China (Grant no. Y6100234) and SRF for ROCS, SEM. J.S. acknowledges the support from NSFC (Grant no. 11372272). R.C.W. acknowledges the support from NSF (Grant no. DGE-1144245). Y.H. acknowledges the supports from NSF and NSFC.

References

1 R. C. Webb, A. P. Bonifas, A. Behnaz, Y. H. Zhang, K. J. Yu, H. Y. Cheng, M. X. Shi, Z. G. Bian, Z. J. Liu, Y. S. Kim, W. H. Yeo, J. S. Park, J. Z. Song, Y. H. Li, Y. Huang, A. M. Gorbach and J. A. Rogers, *Nat. Mater.*, 2013, **12**, 938.
2 R. A. McFarland, *Biofeedback and Self-Regulation*, 1985, **10**, 255.
3 S. E. Rimm-Kaufman and J. Kagan, *Motivation and Emotion*, 1996, **20**, 63.
4 O. Ley, M. Naghavi, C. Deshpande and B. Prapamcham, *J. Biomech. Eng.*, 2008, **130**, 031012.
5 T. Y. Chuang, Y. S. Yen, J. W. Chiu, R. C. Chan, S. C. Chiang, M. P. Hsiao and L. S. Lee, *Arch. Phys. Med. Rehabil.*, 1997, **78**, 85.
6 L. Janský, V. Vávra, P. Janský, P. Kunc, I. Knížková, D. Jandová and K. Slováček, *J. Therm. Biol.*, 2003, **28**, 429.
7 A. Dittmar, C. Gehin, G. Delhomme, D. Boivin, G. Dumont and C. Mott, *Conf Proc IEEE Eng Med Biol Soc.*, 2006, **1**, 900.
8 W. Chen, S. Dols, S. Bambang Oetomo and L. M. G. Feijs, *Proceedings of the Fifth International Conference on Body Area Networks*, 2010, 188.
9 D. H. Kim, N. Lu, R. Ma, Y. S. Kim, R. H. Kim, S. Wang, J. Wu, S. M. Won, H. Tao, A. Islam, K. J. Yu, T. Kim, R. Chowdhury, M. Ying, L. Xu, M. Li, H. J. Chung, H. Keum, M. McCormick, P. Liu, Y. W. Zhang, F. G. Omenetto, Y. Huang, T. Coleman and J. A. Rogers, *Science*, 2011, **333**, 838.
10 Technical Data Sheet, *Semiconductor Materials*, DuPont Co., Wilmington.
11 Technical Data Sheet, *Solaris(TM)*, PSC A/S, Brønderslev.
12 J. F. Shackelford and W. Alexander, *CRC Materials Science and Engineering Handbook*, CRC Press, Boca Raton, 3rd edn, 2001.
13 H. S. Carslaw and J. C. Jaeger, *Conduction of Heat in Solids*, The Clarendon Press, Oxford, 2nd edn, 1959.
14 C. Lu, Y. Li, J. Song, H. S. Kim, E. Brueckner, B. Fang, K. C. Hwang, Y. Huang, R. G. Nuzzo and J. A. Rogers, *Proc. R. Soc. A*, 2012, **468**, 3215.
15 A. D. Polyanin and A. V. Manzhirov, *Mathematics for Engineers and Scientists*, Chapman & Hall/CRC, New York, 1st edn, 2007.